NANO LETTERS

pubs.acs.org/NanoLett Letter

Highly Tunable Enhancement and Switching of Nonlinear Emission from All-Inorganic Lead Halide Perovskites via Electric Field

Yan Gao,[§] Xiaohong Li,[§] Weiwei Liu,* Xiangyuan Xing, Hua Long, Kai Wang, Bing Wang, and Peixiang Lu*

Cite This: https://doi.org/10.1021/acs.nanolett.1c03142 Read Online

ACCESS | Metrics & More | Article Recommendations | Supporting Information

ABSTRACT: Herein, we demonstrate a highly tunable enhancement and switching of nonlinear emission from all-inorganic metal halide perovskites based on an asymmetrically biased metal−insulator−semiconductor (MIS) structure. We achieve 2 orders of magnitude enhancement of the two-photon-pumped photoluminescence (TPL) from $CsPbBr_3$ microplates with the MIS structure, due to comprehensive effects including localized field effect, trap-filling effect, and collection enhancement. In particular, taking advantage of electric-field-induced passivation/activation of Br vacancies, we realize highly tunable TPL enhancement, ranging from ∼61.2-fold to ∼370.3-fold. Moreover, we demonstrate an efficient modulation of the two-photon-pumped lasing from the MIS structure, which exhibits electric field induced switching with a high on/off ratio of 67:1. This work has opened new avenues for steering carrier transport and nonlinear emission in lead halide perovskites, which shows great promise for realizing high-efficiency and tunable nonlinear nanophotonic devices.

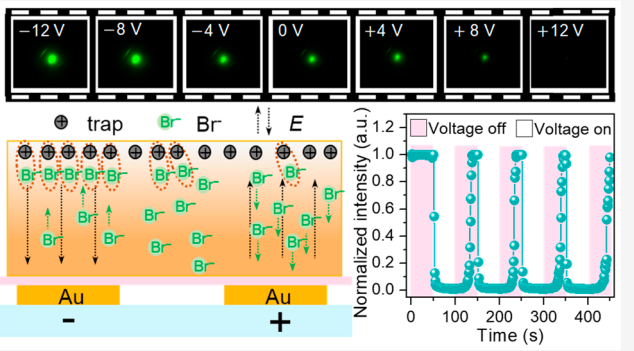

KEYWORDS: *Lead halide perovskites, nonlinear emission, lasing, electric-field modulation, nanophotonics*

INTRODUCTION

Owing to desirable advantages such as large absorption coefficient,[1] tunable optical bandgap,[2] low defect concentration,[3] high defect tolerance,[4−6] and long carrier diffusion length,[7−9] metal halide perovskites show great promise for high-performance optoelectronic devices. Up to now, they have been widely utilized for solar cells,[10−12] nanolasers,[13−15] light-emitting diodes (LEDs), and photodetectors.[16−18] From the outstanding optoelectronic responses, metal halide perovskites have become excellent candidates for nonlinear optics.[19−23] In particular, the two-photon pumped regime exhibits relatively high efficiency, deep penetration, and small damage effect. As a consequence, the nonlinear responses from perovskite materials have attracted great attention in emerging fields, including frequency upconversion,[21,22,24,25] super-resolution imaging,[26] and information processing.[27,28] Moreover, perovskites are highly susceptible to pressure, light, and temperature, which suggests a great tunability of the optical devices.[29−32]

Carrier transport and steering have played important roles for revealing the photophysical processes and modulating the device performances based on perovskites. For example, by combining electric-field-modulated imaging and time-resolved PL spectroscopy, charge transport has been investigated in $CsPbBr_3$ nanoplates.[33] In general, the external electric field would drive the carriers to drift to the opposite directions, leading to a reduction of the PL emission.[34−36] Interestingly, a different mechanism would appear for trap states in the electric field. The nonradiative recombination traps can be passivated by the electric field induced doping, resulting in an increase of the radiative recombination.[37,38] Although the electric field has offered a powerful approach for modulating the optoelectronic responses, the effect on the nonlinear light emission of metal halide perovskites through cooperation with a hybrid structure still remains unexplored, which is especially important for fabricating dynamic and tunable nonlinear nanophotonic devices.

In this work, we demonstrate a highly tunable enhancement and switching of the nonlinear light emission from all-inorganic metal halide perovskites. A hybrid metal−insulator−semiconductor (MIS) structure is fabricated by transferring high-quality $CsPbBr_3$ microplates onto SiO_2-capped Au electrode arrays, which allows for 2 orders of magnitude enhancement of the two-photon-pumped photoluminescence (TPL) of the $CsPbBr_3$ microplates. The TPL enhancement originates from

Received: August 16, 2021
Revised: November 24, 2021

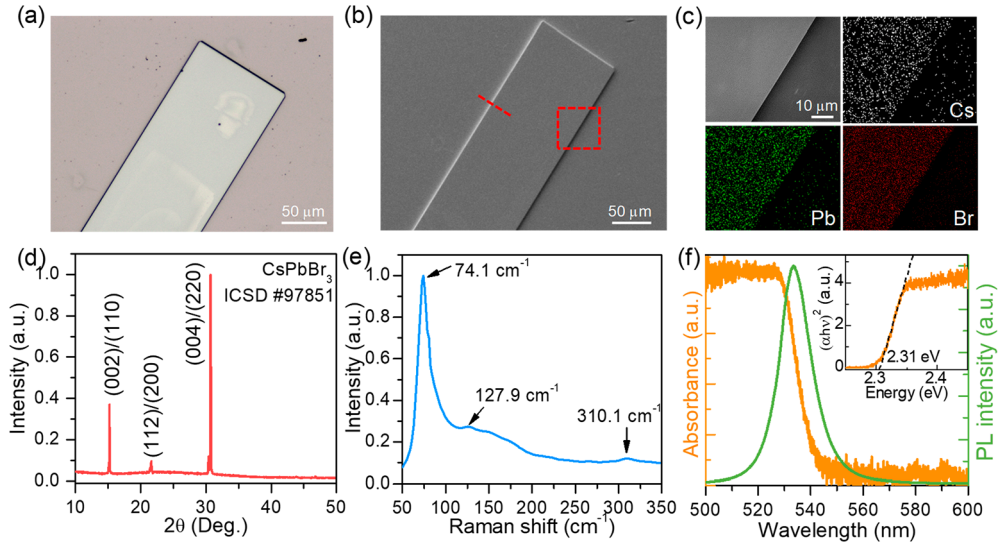

Figure 1. (a) Optical microscopic image and (b) SEM image of an as-grown $CsPbBr_3$ microplate on glass substrate. (c) Elemental analysis, (d) X-ray diffraction pattern, and (e) Raman spectrum of an as-grown $CsPbBr_3$ microplate. (f) Absorption (yellow curve) and two-photon-induced photoluminescence (TPL, green curve) spectra of an as-grown $CsPbBr_3$ microplate. The inset shows the Tauc-plot fitting of the absorption spectrum.

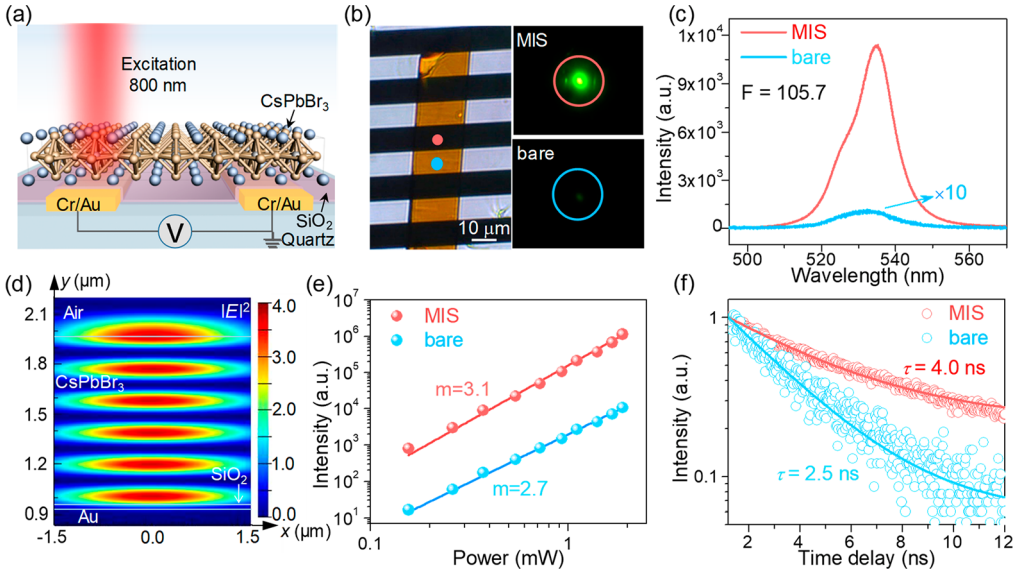

Figure 2. (a) Schematic diagram of the MIS structure composed of vertical-stacking $CsPbBr_3$ microplate, SiO_2 film, and Au electrodes. (b) Left panel: optical microscopic image of the MIS structure. Right panel: dark-field PL images of the MIS structure (upper panel) and bare $CsPbBr_3$ microplate (bottom panel). (c) TPL spectra of the MIS structure (red curve) and the bare $CsPbBr_3$ microplate (blue curve). (d) Simulated electric field distribution in the MIS structure. (e) Plots of the TPL intensity as a function of excitation power for the bare $CsPbBr_3$ microplate (blue dots) and the MIS structure (red dots). The solid curves represent the power-law fitting results. (f) Time-resolved PL decay traces for the bare $CsPbBr_3$ microplate (blue) and the MIS structure (red).

comprehensive effects, including localized field effect, trap-filling effect, and collection enhancement. In particular, the MIS structure facilitates modulation of the nonlinear emission from the $CsPbBr_3$ microplates via electric field, through an asymmetrically biased configuration. Consequently, we realize a highly tunable TPL enhancement ranging from ~61.2-fold to ~370.3-fold by taking advantage of the electric-field-induced passivation/activation of Br vacancies. In addition, we demonstrate an efficient modulation of the two-photon-pumped lasing from the MIS structure with a high on/off ratio of 67:1.

RESULTS AND DISCUSSION

The $CsPbBr_3$ microplates were grown on a 2 × 2 cm^2 glass substrate by using pressure-assisted solution method (Note S1 and Figures S1 and S2, Supporting Information).[25,39] Figure 1a shows the optical microscopic image of an as-grown $CsPbBr_3$ microplate. The lateral size of the microplate is up to several hundred micrometers. The scanning electron microscope (SEM) image in Figure 1b displays a regular shape and smooth surface, indicating a high crystallization quality. The energy dispersive spectroscopy (EDS) results in Figure 1c reveal that Cs, Pb, and Br distribute homogeneously in the microplate (Figure S3, Supporting Information). X-ray

https://doi.org/10.1021/acs.nanolett.1c03142
Nano Lett. XXXX, XXX, XXX−XXX

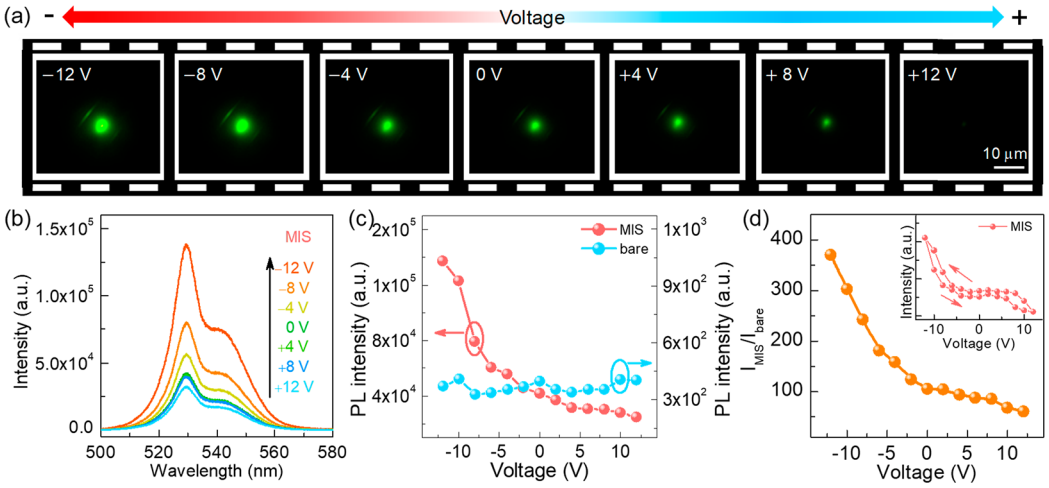

Figure 3. (a) Dark-field PL images of the MIS structure with voltages varying from −12 V to +12 V. (b) Measured TPL spectra with voltages varying from −12 V to +12 V. (c) Plots of TPL intensities versus voltage for the MIS structure (red dots) and bare $CsPbBr_3$ microplate (blue dots). (d) Plot of the TPL enhancement factor of the MIS structure versus voltage. Inset: Reversible electric field modulated TPL in the MIS structure.

diffraction (XRD) characterization displays three sharp diffraction peaks (Figure 1d), and the splitting peaks at (002)/(110), (112)/(200), and (004)/(220) declare the formation of orthorhombic phase. The Raman spectrum in Figure 1e features the inherent mode and interaction between atoms of $CsPbBr_3$, which suggests three active modes corresponding to the Pb−Br vibration of pure $PbBr_6$ octahedron (~74.1 cm^{-1}), the movement of head to head Cs atom combined with adjacent Br face (~127.9 cm^{-1}), and the second-order longitudinal optical (LO) mode (~310.1 cm^{-1}).[40,41] Figure 1f presents the absorption and PL spectra of the $CsPbBr_3$ microplate. A sharp absorption band edge is located at ~532.4 nm, and the bandgap is determined to be ~2.31 eV (inset in Figure 1f), which is in accordance with the reported results.[42]

On the basis of the high-quality $CsPbBr_3$ microplate, a hybrid MIS structure is fabricated by stacking the $CsPbBr_3$ microplate onto a SiO_2-capped Au electrode array, as illustrated in Figure 2a. The clean and smooth surface of the substrate provides a good contact with the $CsPbBr_3$ microplate (Figure S4, Supporting Information). The left panel of Figure 2b presents the microscopic image of the sample, in which the MIS structure and suspended bare $CsPbBr_3$ microplate can be clearly observed. As $CsPbBr_3$ has been demonstrated to exhibit a favorable nonlinear emission,[21,23,43] the hybrid MIS structure would further promote the nonlinear response. For optical measurement, a femtosecond-pulsed Ti:sapphire oscillator centered at 800 nm (Vitara, Coherent) is used as the pumping source. The optical signal is detected by a CCD camera for imaging or by a spectrometer (Andor, SR193i) for spectroscopic measurement (Note S1 and Figure S5, Supporting Information). The right panel of Figure 2b shows the PL images from the MIS structure and bare $CsPbBr_3$ microplate, respectively. Notably, the TPL emission from the MIS structure exhibits a much brighter green spot, indicating a significant enhancement of the signal. Figure 2c shows the corresponding TPL spectra for quantitative characterization. The enhancement factor can be calculated as $F = I_{MIS}/I_0 = 105.7$, where I_{MIS} and I_0 are TPL intensities for the MIS structure and bare $CsPbBr_3$ microplate, respectively.

The giant TPL enhancement can be attributed to the unique hybrid MIS structure. First, the MIS structure can be regarded as a hybrid Fabry−Pérot (F−P) microcavity, thus resulting in a localization enhancement of the excitation. The electric field distribution of the excitation light coupling inside the cavity is calculated by finite-difference time-domain (FDTD) method, as shown in Figure 2d (Note S2 and Figure S6, Supporting Information). The oscillating patterns of the electric field distribution demonstrates the localized-field effect. The average intensity of the excitation field localized inside the microcavity can be calculated as $I_{ave} = \int |E|^2 \, d\nu/V$, with V being the total volume incident by the laser beam, which has been enhanced by ~3.4 times compared with that inside the bare $CsPbBr_3$ microplate. For a third-order nonlinear process, the TPL intensity is proportional to the square of the excitation intensity ($I_{TPL} \sim I_{Ex}^2$), implying ~11.6-fold enhancement of the TPL emission. Second, the enhanced excitation field will produce increased carriers inside the $CsPbBr_3$ microplate, which is beneficial for filling the traps and increasing the radiative recombination of free carriers. For demonstration, the power-dependent TPL intensity was measured, as plotted in Figure 2e. Since both exciton recombination and free carrier recombination exist in the $CsPbBr_3$ perovskite, the experimental results can be well fitted by a power-law model, $I_{TPL} = AI_{Ex}^m$ (Note S3 and Figure S7, Supporting Information).[44,45] In particular, as the excitation power increases, the TPL intensity from the MIS structure grows faster with a slope of ~3.1, indicating an increased proportion of the free carrier recombination (Figure S7, Supporting Information). Previous reports show that the increased free carrier recombination can be attributed to the saturation of the trap-related excitons and dissociation of the free excitons.[44] The increased radiative recombination of the free carriers can also be verified by the increased PL lifetime of the MIS structure (Figure 2f). Besides, the increased reflection of the Au electrode will contribute to an improved collection of the TPL signal. The reflectivity of the TPL signal can be calculated to be 0.36 and 0.175 for the MIS structure and bare $CsPbBr_3$ microplate, respectively, indicating a ~2-fold increase of the TPL collection.

The MIS structure provides a suitable platform to modulate the light emission of the perovskites by external electric field. In the experiment, a direct-current (DC) power supply was connected between the adjacent Au electrodes, as illustrated in Figure 2a. Figure 3a shows the dark-field PL images of the MIS

https://doi.org/10.1021/acs.nanolett.1c03142
Nano Lett. XXXX, XXX, XXX−XXX

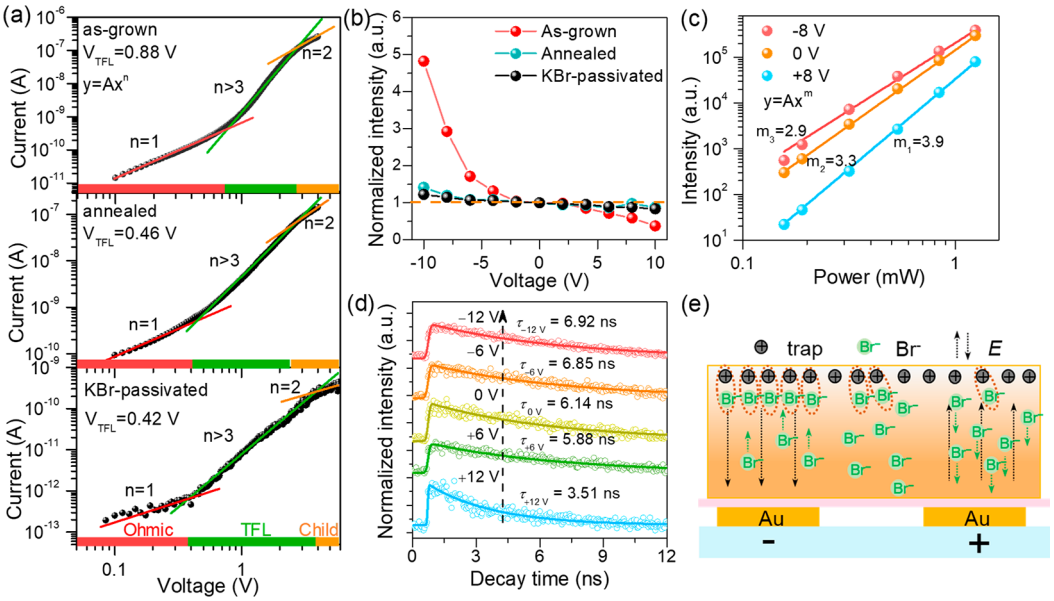

Figure 4. (a) Dark current−voltage (I−V) characteristics of trap density in the as-grown, annealed, and KBr-passivated $CsPbBr_3$ microplates, respectively. (b) Plots of the normalized TPL intensity versus the voltage for the as-prepared (red dots), air-annealed (cyan dots), and KBr-passivated (black dots) MIS structure, respectively. (c) Plots of the TPL intensity as a function of excitation power, with voltages of −8 V (red dots), 0 V (yellow dots), and +8 V (blue dots), respectively. (d) Time-resolved PL decay traces for the MIS structure, with voltages varying from −12 V to +12 V. (e) Schematic illustration of the electri-field-induced interaction between the Br vacancies and excessive Br^-.

structure, with voltages varying from −12 V to +12 V. The "−" ("+") symbol represents that the Au electrode stripe underneath the measured $CsPbBr_3$ microplate is negatively (positively) biased. A maximum voltage of 12 V is adopted to avoid the lattice collapse. Interestingly, the TPL brightness gradually increases as the external bias varies from 0 V to −12 V, while it displays a completely opposite trend when the biased is reversed. Figure 3b plots the corresponding TPL spectra measured at various voltages, which are consistent with the PL images. Figure 3c summarizes the TPL intensity as a function of the biased voltage for the MIS structure and the suspended bare $CsPbBr_3$ microplate. The TPL emission from the MIS structure is strongly dependent on the voltage and polarity of external bias, while that from the bare $CsPbBr_3$ microplate is almost unaffected by the external electric field. The distinct responses to the external electric field suggest different interaction mechanisms of the two parts. The calculated distribution of the imposed electric field shows that the field is vertical to the surface of the MIS structure, while it is parallel to the surface of the $CsPbBr_3$ microplate between the Au electrodes (Note S4 and Figure S8, Supporting Information), revealing that the vertical electric field plays the dominant role in the TPL modulation. More importantly, the vertical electric field is notably asymmetric with respect to the upper and bottom interfaces of the $CsPbBr_3$ microplate, which is responsible for the polarity-dependent TPL emission. Furthermore, we calculate the TPL enhancement in the MIS structure as a function of the biased voltage, as presented in Figure 3d. Overall, the TPL enhancement can be achieved in a highly tunable range by controlling the biased voltage, from ∼61.2 times to ∼370.3 times, which implies a novel effect for engineering the TPL emission (Table S1, Supporting Information). We also noted that similar results can be observed in the MIS structure with $CsPbBr_3$ films (Note S5 and Figure S9, Supporting Information). In addition, the electric field modulated TPL emission possesses a great reversibility (inset of Figure 3d), suggesting an excellent stability of the $CsPbBr_3$ microplates under the external bias.

Generally, the external electric field will drive the electrons and holes to separate, which leads to a decrease of the recombination rate.[46] Actually, the electric field can also drive the motion of charged particles, such as the electron/hole traps.[47] As reported, the trap density is in the range 10^{10}−10^{18} cm^{-3} in lead halide perovskites.[44,48] To investigate whether the traps have effect on the electric field modulated TPL, the $CsPbBr_3$ perovskite is processed to reduce the trap density by using annealing treatment[49,50] and potassium passivation[51] (Note S6 and Figures S10 and S11, Supporting Information). The trap density can be characterized by the space-charge-limited current method.[52−55] As shown in Figure 4a, the trap-filled limit voltage (V_{TFL}) is determined to be ∼0.88 V, ∼0.46 V, and ∼0.42 V, respectively, for the as-grown, annealed, and KBr-passivated $CsPbBr_3$ microplates. Correspondingly, the trap density is calculated as[53,54]

$$N_t = \frac{2\varepsilon_0\varepsilon_r V_{TFL}}{eL^2} \quad (1)$$

where ε_0 is the vacuum permittivity. ε_r is the relative dielectric constant of $CsPbBr_3$ crystal (ε_r = 22).[54] e is the elemental charge, and L is the distance between the electrodes (L = 10 μm). With this method, the trap density of the as-grown $CsPbBr_3$ microplate is measured to be ∼2.1 × 10^{13} cm^{-3}, which reduces to ∼1.1 × 10^{13} cm^{-3} and ∼1.0 × 10^{13} cm^{-3} after the annealing treatment and potassium passivation, respectively. And then we measured electric field modulated TPL emission of the MIS structures with trap-reduced $CsPbBr_3$ microplates to compare with the as-prepared samples, as shown in Figure 4b. In this situation, the TPL intensity has a slight variation as the voltage changes from −10 V to +10 V, which is significantly distinct from the as-prepared MIS structure. Therefore, we can conclude that the traps in the

https://doi.org/10.1021/acs.nanolett.1c03142
Nano Lett. XXXX, XXX, XXX−XXX

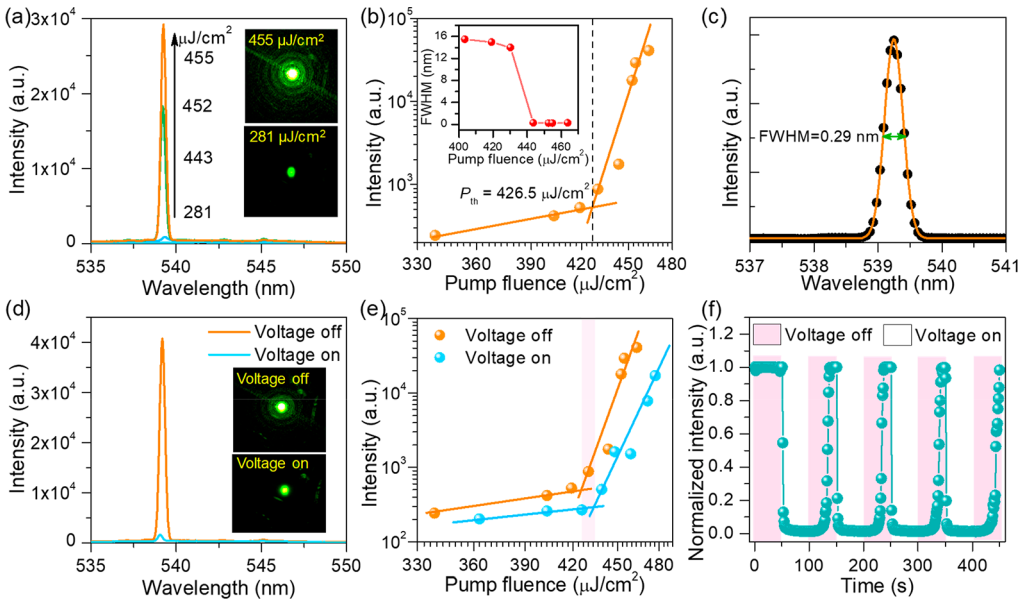

Figure 5. (a) Plot of TPL spectrum of the MIS structure versus pump fluence. Inset: PL images below (281 μJ/cm^2) and beyond (455 μJ/cm^2) lasing threshold. (b) The log−log plot of the peak density versus the pump fluence. Inset: Corresponding fwhm of the spectrum versus the pump fluence. (c) Typical lasing spectrum of the MIS structure, showing a fwhm of ∼0.29 nm. (d) Lasing spectra of the MIS structure with voltage on (blue curve) and voltage off (yellow curve). Insets present the corresponding dark-field PL images. (e) The log−log plot of lasing intensity versus the pump fluence, with voltage on (blue dots) and voltage off (yellow dots). (f) Dynamic switching characteristic of the lasing emission.

as-grown $CsPbBr_3$ perovskite play a dominant role in the electric-field modulated TPL emission.

Taking the traps into consideration, the two-photon pumped recombination dynamics can be described by the following rate equations (Note S3, Supporting Information)[56,57]

$$\frac{dn}{dt} = G - k_b np - k_t(N_t - n_t)n \quad (2)$$

$$\frac{dp}{dt} = G - k_b np - k_h k_t p \quad (3)$$

$$\frac{dn_t}{dt} = k_t(N_t - n_t)n - k_h k_t p \quad (4)$$

where n (p) represents the electron (hole) concentration. n_t is the trapped electron concentration, and N_t represents the total trap concentration. k_b, k_t, and k_h represent the electron−hole recombination rate, the electron trapping rate, and the electron detrapping rate, respectively. G represents the generation rate of electrons (holes), $G = (I_{exc}/(h\nu))^2\sigma_{2P}$, with σ_{2P} being the two-photon absorption cross section.[56] We measured the power-dependent TPL of the MIS structure at different voltages (Figure 4c), which can be numerically fitted by solving the rate equations 1−3 with the Runge−Kutta method. The TPL intensity exhibits a power-law dependence on the excitation power, and the slope values are obtained to be 3.9, 3.3, and 2.9 for the +8 V, 0 V, and −8 V biased situations, respectively, corresponding to a gradually decreased total trap concentration (N_t) in the $CsPbBr_3$ microplate (Figure S7, Supporting Information). Moreover, the time-resolved PL decays shown in Figure 4d indicate that as the biased voltage varies from +12 V to −12 V, the PL lifetime increases from 3.51 to 6.92 ns, which further demonstrates the decreased nonradiative recombination with a negative-biased electric field.[58]

In order to understand the underlying mechanism, the characteristics of the electric field modulated TPL emission of the MIS structure can be summarized as follows: (1) The traps in the $CsPbBr_3$ microplate play important roles. (2) Only the vertical electric field is effective for the TPL modulation. (3) The interaction process is strongly dependent on the polarity of the vertical electric field, and a negatively biased electric field is advantageous for decreasing the traps. Combined with the above analyses, a phenomenological model is proposed to illustrate the interaction process, as schemed in Figure 4e. As the halogen vacancies represent the most common trap state in the halides, Br vacancies (V_{Br}^+) are considered to mainly exist at the surface of the $CsPbBr_3$ microplate, which act as the positive center and can capture the photogenerated electrons.[51] Elementary analysis indicates that the Br element is slightly excessive in the as-grown $CsPbBr_3$ microplate (Figure S3, Supporting Information). With negative-biased electric field, the excessive Br^- will travel toward to the upper surface of the $CsPbBr_3$ microplate, thus resulting in a Br-rich distribution at the surface. The Br-rich distribution is beneficial for passivating the traps induced by the Br vacancies and increasing the proportion of the radiative recombination.[51] As a consequence, the TPL emission can get enlarged. In contrast, with a positive-biased electric field, Br^- will move to the bottom interface of the $CsPbBr_3$ microplate. Correspondingly, Br vacancies near the upper surface of the $CsPbBr_3$ microplate are further increased, resulting in a decrease of the TPL emission. For further demonstration, we prepared the MIS samples with Pb-rich $CsPbBr_3$ microplate to measure the TPL emission. The TPL intensity is decreased for both the negatively and positively biased electric field (Figure S12, Supporting Information), indicating that the excessive Pb^{2+} has no effect on repairing the traps in the $CsPbBr_3$ microplate. Therefore, we can conclude that the Br vacancies are the dominant electron traps in the as-grown $CsPbBr_3$ microplate,

https://doi.org/10.1021/acs.nanolett.1c03142
Nano Lett. XXXX, XXX, XXX−XXX

and the electric field modulated TPL emission originates from the interaction between the Br vacancies and excessive Br^-.

As the MIS structure can be regarded as a hybrid F−P microcavity, it offers a versatile system for us to investigate the field-modulated lasing behavior. For lasing measurements, the femtosecond pulses from a Ti:sapphire regenerative amplifier centered at 800 nm were used as the excitation source. Figure 5a shows the TPL spectrum of the MIS structure versus the pump fluence. As the pump fluence increases from 281 $\mu J/cm^2$ to 455 $\mu J/cm^2$, the TPL intensity exhibits a sharp increase and the PL image varies from a homogeneous spot to a coherent diffraction pattern (inset of Figure 5a), which demonstrate the occurrence of stimulated emission. Moreover, the log−log plot of the TPL intensity versus the pump fluence shows the "kink" characteristic (Figure 5b), representing a typical feature for the transition from spontaneous emission to stimulated emission. Correspondingly, the fwhm of the PL spectra experiences a dramatic decrease (inset of Figure 5b). The transition of spontaneous emission toward stimulated emission occurs at P = 426.5 $\mu J/cm^2$, which is determined as the lasing threshold. Figure 5c shows that the lasing line width (fwhm) is fitted to be $\Delta\lambda$ = 0.29 nm. Therefore, the quality factor of the lasing emission can be calculated as $Q = \lambda/\Delta\lambda$ = 1866. We further investigate the lasing characteristics, which exhibit excellent performance (Note S7, Figure S13, and Table S2, Supporting Information).

The electric field effect on the lasing emission is investigated by applying a biased voltage on the MIS structure. Figure 5d shows the lasing spectra of the MIS structure at a pump fluence of 462 $\mu J/cm^2$, with (−12 V) and without (0 V) the external bias. Differing from the TPL regime, the lasing intensity has been strongly attenuated once the −12 V voltage is imposed on the sample. We also measure the power-dependent TPL intensity, as shown in Figure 5e. The threshold of the two-photon pumped lasing is slightly increased under the −12 V bias (~435 $\mu J/cm^2$). A previous report indicates that the lasing behavior in $CsPbBr_3$ is dominantly originating from the stimulated emission of electron−hole plasma (EHP).[59] Although the surface traps have played an important role in the electric field modulated TPL emission, the effect on the lasing emission can be screened by the high-density electron−hole plasma. Therefore, the damping of the lasing behavior under external bias is ascribed to the destruction of the electron−hole correlation. As further evidence, the lasing emission is no longer dependent on the polarity of the external electric field because similar results can be obtained for both the positive bias and negative bias (Figure S14, Supporting Information). In order to realize a dynamical tuning of the lasing behavior, the external bias is turned on and off alternatively for every 50 s. Correspondingly, the lasing emission experiences a periodic switching between the on/off states, as displayed in Figure 5f. The on/off ratio, defined as the ratio between the lasing intensities at 0 and 12 V, is determined to be 67:1, which suggests a high performance of the electric-field-induced modulation.

CONCLUSION

In summary, we have demonstrated highly tunable TPL enhancement and lasing switching of the $CsPbBr_3$ microplates based on the MIS structure. The MIS structure has promoted a 105.7-fold enhancement of the TPL from the $CsPbBr_3$ microplate, due to comprehensive effects including field localization effect, trap-filling effect, and increased collection efficiency. Moreover, the TPL emission can be modulated by an external electric field, and a highly tunable TPL enhancement from ~61.2 to ~370.3 times has been achieved, which is attributed to electric-field-induced passivation/activation of Br vacancies in the $CsPbBr_3$ microplate. Besides, an efficient switching of the two-photon-pumped lasing from the MIS structure has been demonstrated. This work has opened new avenues for steering the carrier transport and nonlinear light emission in lead halide perovskites, which shows great promise for realizing high-efficiency and tunable nonlinear nanophotonic devices.

ASSOCIATED CONTENT

Supporting Information

The Supporting Information is available free of charge at https://pubs.acs.org/doi/10.1021/acs.nanolett.1c03142.

Sample fabrication details, experiment setup, the dynamic model of TPL emission process, electric-field modulated lasing behavior, and additional experimental and simulation results (PDF)

AUTHOR INFORMATION

Corresponding Authors

Weiwei Liu − *Wuhan National Laboratory for Optoelectronics and School of Physics, Huazhong University of Science and Technology, Wuhan 430074, China;* orcid.org/0000-0001-9451-1968; Email: lwhust@hust.edu.cn

Peixiang Lu − *Wuhan National Laboratory for Optoelectronics and School of Physics, Huazhong University of Science and Technology, Wuhan 430074, China; Hubei Key Laboratory of Optical Information and Pattern Recognition, Wuhan Institute of Technology, Wuhan 430205, China;* Email: lupeixiang@hust.edu.cn

Authors

Yan Gao − *Wuhan National Laboratory for Optoelectronics and School of Physics, Huazhong University of Science and Technology, Wuhan 430074, China*

Xiaohong Li − *Hubei Key Laboratory of Optical Information and Pattern Recognition, Wuhan Institute of Technology, Wuhan 430205, China*

Xiangyuan Xing − *Wuhan National Laboratory for Optoelectronics and School of Physics, Huazhong University of Science and Technology, Wuhan 430074, China*

Hua Long − *Wuhan National Laboratory for Optoelectronics and School of Physics, Huazhong University of Science and Technology, Wuhan 430074, China*

Kai Wang − *Wuhan National Laboratory for Optoelectronics and School of Physics, Huazhong University of Science and Technology, Wuhan 430074, China*

Bing Wang − *Wuhan National Laboratory for Optoelectronics and School of Physics, Huazhong University of Science and Technology, Wuhan 430074, China*

Complete contact information is available at: https://pubs.acs.org/10.1021/acs.nanolett.1c03142

Author Contributions

[§]Y.G. and X.L. contributed equally to this work.

Notes

The authors declare no competing financial interest.

https://doi.org/10.1021/acs.nanolett.1c03142
Nano Lett. XXXX, XXX, XXX−XXX

■ ACKNOWLEDGMENTS

This work was financially supported by the National Natural Science Foundation of China (Grants 11804109 and 11674117) and The National Natural Science Foundation of China for Innovative Research Groups (Grant 12021004). We acknowledge the Analytical & Testing Center of Huazhong University of Science and Technology (HUST) for XRD measurements, and the Center of Micro-Fabrication and Characterization (CMFC) of WNLO for the support in step profiler measurements.

■ REFERENCES

(1) Manser, J. S.; Christians, J. A.; Kamat, P. V. Intriguing Optoelectronic Properties of Metal Halide Perovskites. *Chem. Rev.* **2016**, *116* (21), 12956−13008.
(2) Sutherland, B. R.; Sargent, E. H. Perovskite Photonic Sources. *Nat. Photonics* **2016**, *10* (5), 295−302.
(3) Kumar, A.; Solanki, A.; Manjappa, M.; Ramesh, S.; Srivastava, Y. K.; Agarwal, P.; Sum, T. C.; Singh, R. Excitons in 2D Perovskites for Ultrafast Terahertz Photonic Devices. *Sci. Adv.* **2020**, *6* (8), No. eaax8821.
(4) Kang, J.; Wang, L.-W. High Defect Tolerance in Lead Halide Perovskite $CsPbBr_3$. *J. Phys. Chem. Lett.* **2017**, *8* (2), 489−493.
(5) Steirer, K. X.; Schulz, P.; Teeter, G.; Stevanovic, V.; Yang, M.; Zhu, K.; Berry, J. J. Defect Tolerance in Methylammonium Lead Triiodide Perovskite. *ACS Energy Lett.* **2016**, *1* (2), 360−366.
(6) Tan, H.; Che, F.; Wei, M.; Zhao, Y.; Saidaminov, M. I.; Todorović, P.; Broberg, D.; Walters, G.; Tan, F.; Zhuang, T.; Sun, B.; Liang, Z.; Yuan, H.; Fron, E.; Kim, J.; Yang, Z.; Voznyy, O.; Asta, M.; Sargent, E. H. Dipolar Cations Confer Defect Tolerance in Wide-Bandgap Metal Halide Perovskites. *Nat. Commun.* **2018**, *9* (1), 3100.
(7) Stranks, S. D.; Eperon, G. E.; Grancini, G.; Menelaou, C.; Alcocer, M. J. P.; Leijtens, T.; Herz, L. M.; Petrozza, A.; Snaith, H. J. Electron-Hole Diffusion Lengths Exceeding 1 Micrometer in an Organometal Trihalide Perovskite Absorber. *Science* **2013**, *342* (6156), 341−344.
(8) Yettapu, G. R.; Talukdar, D.; Sarkar, S.; Swarnkar, A.; Nag, A.; Ghosh, P.; Mandal, P. Terahertz Conductivity within Colloidal $CsPbBr_3$ Perovskite Nanocrystals: Remarkably High Carrier Mobilities and Large Diffusion Lengths. *Nano Lett.* **2016**, *16* (8), 4838−4848.
(9) Xing, G.; Mathews, N.; Sun, S.; Lim, S. S.; Lam, Y. M.; Grätzel, M.; Mhaisalkar, S.; Sum, T. C. Long-Range Balanced Electron- and Hole-Transport Lengths in Organic-Inorganic $CH_3NH_3PbI_3$. *Science* **2013**, *342* (6156), 344−347.
(10) Correa-Baena, J.-P.; Saliba, M.; Buonassisi, T.; Grätzel, M.; Abate, A.; Tress, W.; Hagfeldt, A. Promises and Challenges of Perovskite Solar Cells. *Science* **2017**, *358* (6364), 739−744.
(11) Bi, D.; Li, X.; Milić, J. V.; Kubicki, D. J.; Pellet, N.; Luo, J.; LaGrange, T.; Mettraux, P.; Emsley, L.; Zakeeruddin, S. M.; Grätzel, M. Multifunctional Molecular Modulators for Perovskite Solar Cells with over 20% Efficiency and High Operational Stability. *Nat. Commun.* **2018**, *9* (1), 4482.
(12) Yoo, J. J.; Seo, G.; Chua, M. R.; Park, T. G.; Lu, Y.; Rotermund, F.; Kim, Y.-K.; Moon, C. S.; Jeon, N. J.; Correa-Baena, J.-P.; Bulović, V.; Shin, S. S.; Bawendi, M. G.; Seo, J. Efficient Perovskite Solar Cells Via Improved Carrier Management. *Nature* **2021**, *590* (7847), 587−593.
(13) Zhu, H.; Fu, Y.; Meng, F.; Wu, X.; Gong, Z.; Ding, Q.; Gustafsson, M. V.; Trinh, M. T.; Jin, S.; Zhu, X. Y. Lead Halide Perovskite Nanowire Lasers with Low Lasing Thresholds and High Quality Factors. *Nat. Mater.* **2015**, *14*, 636−642.
(14) Shang, Q.; Li, M.; Zhao, L.; Chen, D.; Zhang, S.; Chen, S.; Gao, P.; Shen, C.; Xing, J.; Xing, G.; Shen, B.; Liu, X.; Zhang, Q. Role of the Exciton-Polariton in a Continuous-Wave Optically Pumped $CsPbBr_3$ Perovskite Laser. *Nano Lett.* **2020**, *20* (9), 6636−6643.
(15) Zhang, Q.; Shang, Q.; Su, R.; Do, T. T. H.; Xiong, Q. Halide Perovskite Semiconductor Lasers: Materials, Cavity Design, and Low Threshold. *Nano Lett.* **2021**, *21* (5), 1903−1914.
(16) Chen, C.; Han, T.-H.; Tan, S.; Xue, J.; Zhao, Y.; Liu, Y.; Wang, H.; Hu, W.; Bao, C.; Mazzeo, M.; Wang, R.; Duan, Y.; Yang, Y. Efficient Flexible Inorganic Perovskite Light-Emitting Diodes Fabricated with $CsPbBr_3$ Emitters Prepared Via Low-Temperature in Situ Dynamic Thermal Crystallization. *Nano Lett.* **2020**, *20* (6), 4673−4680.
(17) Fu, Y.; Zhu, H.; Chen, J.; Hautzinger, M. P.; Zhu, X. Y.; Jin, S. Metal Halide Perovskite Nanostructures for Optoelectronic Applications and the Study of Physical Properties. *Nat. Rev. Mater.* **2019**, *4* (3), 169−188.
(18) Stranks, S. D.; Snaith, H. J. Metal-Halide Perovskites for Photovoltaic and Light-Emitting Devices. *Nat. Nanotechnol.* **2015**, *10*, 391−402.
(19) Xu, J. L.; Li, X. Y.; Xiong, J. B.; Yuan, C. Q.; Semin, S.; Rasing, T.; Bu, X. H. Halide Perovskites for Nonlinear Optics. *Adv. Mater.* **2020**, *32* (3), 1806736.
(20) Saouma, F. O.; Stoumpos, C. C.; Wong, J.; Kanatzidis, M. G.; Jang, J. I. Selective Enhancement of Optical Nonlinearity in Two-Dimensional Organic-Inorganic Lead Iodide Perovskites. *Nat. Commun.* **2017**, *8*, 742.
(21) Xu, Y. Q.; Chen, Q.; Zhang, C. F.; Wang, R.; Wu, H.; Zhang, X. Y.; Xing, G. C.; Yu, W. W.; Wang, X. Y.; Zhang, Y.; Xiao, M. Two-Photon-Pumped Perovskite Semiconductor Nanocrystal Lasers. *J. Am. Chem. Soc.* **2016**, *138* (11), 3761−3768.
(22) Wang, Y.; Li, X. M.; Zhao, X.; Xiao, L.; Zeng, H. B.; Sun, H. D. Nonlinear Absorption and Low-Threshold Multiphoton Pumped Stimulated Emission from All-Inorganic Perovskite Nanocrystals. *Nano Lett.* **2016**, *16* (1), 448−453.
(23) Becker, C.; Burger, S.; Barth, C.; Manley, P.; Jäger, K.; Eisenhauer, D.; Köppel, G.; Chabera, P.; Chen, J.; Zheng, K.; Pullerits, T. Nanophotonic-Enhanced Two-Photon-Excited Photoluminescence of Perovskite Quantum Dots. *ACS Photonics* **2018**, *5* (11), 4668−4676.
(24) Liu, Z. Z.; Yang, J.; Du, J.; Hu, Z. P.; Shi, T. C.; Zhang, Z. Y.; Liu, Y. Q.; Tang, X. S.; Leng, Y. X.; Li, R. X. Robust Subwavelength Single-Mode Perovskite Nanocuboid Laser. *ACS Nano* **2018**, *12* (6), 5923−5931.
(25) Li, X. H.; Liu, W. W.; Song, Y. L.; Long, H.; Wang, K.; Wang, B.; Lu, P. X. Two-Photon-Pumped High-Quality, Single-Mode Vertical Cavity Lasing Based on Perovskite Monocrystalline Films. *Nano Energy* **2020**, *68*, 104334.
(26) Liu, W.; Li, X.; Song, Y.; Zhang, C.; Han, X.; Long, H.; Wang, B.; Wang, K.; Lu, P. Cooperative Enhancement of Two-Photon-Absorption-Induced Photoluminescence from a 2D Perovskite-Microsphere Hybrid Dielectric Structure. *Adv. Funct. Mater.* **2018**, *28* (26), 1707550.
(27) Fan, Y. B.; Wang, Y. H.; Zhang, N.; Sun, W. Z.; Gao, Y. S.; Qiu, C. W.; Song, Q. H.; Xiao, S. M. Resonance-Enhanced Three-Photon Luminesce Via Lead Halide Perovskite Metasurfaces for Optical Encoding. *Nat. Commun.* **2019**, *10*, 2085.
(28) Walters, G.; Sutherland, B. R.; Hoogland, S.; Shi, D.; Comin, R.; Sellan, D. P.; Bakr, O. M.; Sargent, E. H. Two-Photon Absorption in Organometallic Bromide Perovskites. *ACS Nano* **2015**, *9* (9), 9340−9346.
(29) Song, Y.; Liu, W.; Qin, Y.; Han, X.; Li, W.; Li, X.; Long, H.; Li, D.; Wang, K.; Wang, B.; Lu, P. Photoinduced Trap Passivation for Enhanced Photoluminescence in 2D Organic−Inorganic Hybrid Perovskites. *Adv. Opt. Mater.* **2020**, *8* (7), 1901695.
(30) Ummadisingu, A.; Steier, L.; Seo, J.-Y.; Matsui, T.; Abate, A.; Tress, W.; Grätzel, M. The Effect of Illumination on the Formation of Metal Halide Perovskite Films. *Nature* **2017**, *545* (7653), 208−212.
(31) Lin, C.-K.; Zhao, Q.; Zhang, Y.; Cestellos-Blanco, S.; Kong, Q.; Lai, M.; Kang, J.; Yang, P. Two-Step Patterning of Scalable All-Inorganic Halide Perovskite Arrays. *ACS Nano* **2020**, *14* (3), 3500−3508.

https://doi.org/10.1021/acs.nanolett.1c03142
Nano Lett. XXXX, XXX, XXX−XXX

(32) Liu, S.; Sun, S.; Gan, C. K.; del Águila, A. G.; Fang, Y.; Xing, J.; Do, T. T. H.; White, T. J.; Li, H.; Huang, W.; Xiong, Q. Manipulating Efficient Light Emission in Two-Dimensional Perovskite Crystals by Pressure-Induced Anisotropic Deformation. *Sci. Adv.* **2019**, *5* (7), No. eaav9445.
(33) Hu, X.; Wang, X.; Fan, P.; Li, Y.; Zhang, X.; Liu, Q.; Zheng, W.; Xu, G.; Wang, X.; Zhu, X.; Pan, A. Visualizing Carrier Transport in Metal Halide Perovskite Nanoplates Via Electric Field Modulated Photoluminescence Imaging. *Nano Lett.* **2018**, *18* (5), 3024−3031.
(34) Wang, Z.; Liu, J.; Xu, Z.-Q.; Xue, Y.; Jiang, L.; Song, J.; Huang, F.; Wang, Y.; Zhong, Y. L.; Zhang, Y.; Cheng, Y.-B.; Bao, Q. Wavelength-Tunable Waveguides Based on Polycrystalline Organic−Inorganic Perovskite Microwires. *Nanoscale* **2016**, *8* (12), 6258−6264.
(35) Yuan, F.; Wu, Z.; Dong, H.; Xia, B.; Xi, J.; Ning, S.; Ma, L.; Hou, X. Electric Field-Modulated Amplified Spontaneous Emission in Organo-Lead Halide Perovskite $Ch_3nh_3pbi_3$. *Appl. Phys. Lett.* **2015**, *107* (26), 261106.
(36) Leijtens, T.; Srimath Kandada, A. R.; Eperon, G. E.; Grancini, G.; D'Innocenzo, V.; Ball, J. M.; Stranks, S. D.; Snaith, H. J.; Petrozza, A. Modulating the Electron−Hole Interaction in a Hybrid Lead Halide Perovskite with an Electric Field. *J. Am. Chem. Soc.* **2015**, *137* (49), 15451−15459.
(37) Yi, H. T.; Rangan, S.; Tang, B.; Frisbie, C. D.; Bartynski, R. A.; Gartstein, Y. N.; Podzorov, V. Electric-Field Effect on Photoluminescence of Lead-Halide Perovskites. *Mater. Today* **2019**, *28*, 31−39.
(38) Xing, J.; Zhao, C.; Zou, Y.; Kong, W.; Yu, Z.; Shan, Y.; Dong, Q.; Zhou, D.; Yu, W.; Guo, C. Modulating the Optical and Electrical Properties of $MAPbBr_3$ Single Crystals Via Voltage Regulation Engineering and Application in Memristors. *Light: Sci. Appl.* **2020**, *9* (1), 111.
(39) Yang, Z.; Xu, Q.; Wang, X.; Lu, J.; Wang, H.; Li, F.; Zhang, L.; Hu, G.; Pan, C. Large and Ultrastable All-Inorganic $CsPbBr_3$ Monocrystalline Films: Low-Temperature Growth and Application for High-Performance Photodetectors. *Adv. Mater.* **2018**, *30* (44), 1802110.
(40) Yaffe, O.; Guo, Y.; Tan, L. Z.; Egger, D. A.; Hull, T.; Stoumpos, C. C.; Zheng, F.; Heinz, T. F.; Kronik, L.; Kanatzidis, M. G.; Owen, J. S.; Rappe, A. M.; Pimenta, M. A.; Brus, L. E. Local Polar Fluctuations in Lead Halide Perovskite Crystals. *Phys. Rev. Lett.* **2017**, *118* (13), 136001.
(41) Zhao, L.; Gao, Y.; Su, M.; Shang, Q.; Liu, Z.; Li, Q.; Wei, Q.; Li, M.; Fu, L.; Zhong, Y.; Shi, J.; Chen, J.; Zhao, Y.; Qiu, X.; Liu, X.; Tang, N.; Xing, G.; Wang, X.; Shen, B.; Zhang, Q. Vapor-Phase Incommensurate Heteroepitaxy of Oriented Single-Crystal $CsPbBr_3$ on Gan: Toward Integrated Optoelectronic Applications. *ACS Nano* **2019**, *13* (9), 10085−10094.
(42) Yang, B.; Zhang, F.; Chen, J.; Yang, S.; Xia, X.; Pullerits, T.; Deng, W.; Han, K. Ultrasensitive and Fast All-Inorganic Perovskite-Based Photodetector Via Fast Carrier Diffusion. *Adv. Mater.* **2017**, *29* (40), 1703758.
(43) Chen, W.; Bhaumik, S.; Veldhuis, S. A.; Xing, G.; Xu, Q.; Gratzel, M.; Mhaisalkar, S.; Mathews, N.; Sum, T. C. Giant Five-Photon Absorption from Multidimensional Core-Shell Halide Perovskite Colloidal Nanocrystals. *Nat. Commun.* **2017**, *8*, 15198.
(44) Zhong, Y.; Liao, K.; Du, W.; Zhu, J.; Shang, Q.; Zhou, F.; Wu, X.; Sui, X.; Shi, J.; Yue, S.; Wang, Q.; Zhang, Y.; Zhang, Q.; Hu, X.; Liu, X. Large-Scale Thin $CsPbBr_3$ Single-Crystal Film Grown on Sapphire Via Chemical Vapor Deposition: Toward Laser Array Application. *ACS Nano* **2020**, *14* (11), 15605−15615.
(45) Zhu, H.; Trinh, M. T.; Wang, J.; Fu, Y.; Joshi, P. P.; Miyata, K.; Jin, S.; Zhu, X. Y. Organic Cations Might Not Be Essential to the Remarkable Properties of Band Edge Carriers in Lead Halide Perovskites. *Adv. Mater.* **2017**, *29* (1), 1603072.
(46) Yang, X.; Shan, Z.; Luo, Z.; Hu, X.; Liu, H.; Liu, Q.; Zhang, Y.; Zhang, X.; Shoaib, M.; Qu, J.; Yi, X.; Wang, X.; Zhu, X.; Liu, Y.; Liao, L.; Wang, X.; Chen, S.; Pan, A. An Electrically Controlled Wavelength-Tunable Nanoribbon Laser. *ACS Nano* **2020**, *14* (3), 3397−3404.
(47) Li, C.; Guerrero, A.; Huettner, S.; Bisquert, J. Unravelling the Role of Vacancies in Lead Halide Perovskite through Electrical Switching of Photoluminescence. *Nat. Commun.* **2018**, *9*, 5113.
(48) Ni, Z.; Bao, C.; Liu, Y.; Jiang, Q.; Wu, W.-Q.; Chen, S.; Dai, X.; Chen, B.; Hartweg, B.; Yu, Z.; Holman, Z.; Huang, J. Resolving Spatial and Energetic Distributions of Trap States in Metal Halide Perovskite Solar Cells. *Science* **2020**, *367* (6484), 1352−1358.
(49) Dualeh, A.; Tetreault, N.; Moehl, T.; Gao, P.; Nazeeruddin, M. K.; Gratzel, M. Effect of Annealing Temperature on Film Morphology of Organic-Inorganic Hybrid Pervoskite Solid-State Solar Cells. *Adv. Funct. Mater.* **2014**, *24* (21), 3250−3258.
(50) Zhao, X. M.; Liu, T. R.; Kaplan, A. B.; Yao, C.; Loo, Y. L. Accessing Highly Oriented Two-Dimensional Perovskite Films Via Solvent-Vapor Annealing for Efficient and Stable Solar Cells. *Nano Lett.* **2020**, *20* (12), 8880−8889.
(51) Abdi-Jalebi, M.; Andaji-Garmaroudi, Z.; Cacovich, S.; Stavrakas, C.; Philippe, B.; Richter, J. M.; Alsari, M.; Booker, E. P.; Hutter, E. M.; Pearson, A. J.; Lilliu, S.; Savenije, T. J.; Rensmo, H.; Divitini, G.; Ducati, C.; Friend, R. H.; Stranks, S. D. Maximizing and Stabilizing Luminescence from Halide Perovskites with Potassium Passivation. *Nature* **2018**, *555*, 497−501.
(52) Chen, Y.; Lei, Y.; Li, Y.; Yu, Y.; Cai, J.; Chiu, M.-H.; Rao, R.; Gu, Y.; Wang, C.; Choi, W.; Hu, H.; Wang, C.; Li, Y.; Song, J.; Zhang, J.; Qi, B.; Lin, M.; Zhang, Z.; Islam, A. E.; Maruyama, B.; Dayeh, S.; Li, L.-J.; Yang, K.; Lo, Y.-H.; Xu, S. Strain Engineering and Epitaxial Stabilization of Halide Perovskites. *Nature* **2020**, *577* (7789), 209−215.
(53) Zhao, X.; Yao, C.; Liu, T.; Hamill, J. C., Jr; Ngongang Ndjawa, G. O.; Cheng, G.; Yao, N.; Meng, H.; Loo, Y.-L. Extending the Photovoltaic Response of Perovskite Solar Cells into the near-Infrared with a Narrow-Bandgap Organic Semiconductor. *Adv. Mater.* **2019**, *31* (49), 1904494.
(54) Zeng, J.; Li, X.; Wu, Y.; Yang, D.; Sun, Z.; Song, Z.; Wang, H.; Zeng, H. Space-Confined Growth of $CsPbBr_3$ Film Achieving Photodetectors with High Performance in All Figures of Merit. *Adv. Funct. Mater.* **2018**, *28* (43), 1804394.
(55) Gao, L.; Zeng, K.; Guo, J.; Ge, C.; Du, J.; Zhao, Y.; Chen, C.; Deng, H.; He, Y.; Song, H.; Niu, G.; Tang, J. Passivated Single-Crystalline $CH_3NH_3PbI_3$ Nanowire Photodetector with High Detectivity and Polarization Sensitivity. *Nano Lett.* **2016**, *16* (12), 7446−7454.
(56) Wang, X.; Zhuang, X.; Wackenhut, F.; Li, Y.; Pan, A.; Meixner, A. J. Power- and Polarization Dependence of Two Photon Luminescence of Single Cdse Nanowires with Tightly Focused Cylindrical Vector Beams of Ultrashort Laser Pulses. *Laser Photon. Rev.* **2016**, *10* (5), 835−842.
(57) Draguta, S.; Thakur, S.; Morozov, Y. V.; Wang, Y.; Manser, J. S.; Kamat, P. V.; Kuno, M. Spatially Non-Uniform Trap State Densities in Solution-Processed Hybrid Perovskite Thin Films. *J. Phys. Chem. Lett.* **2016**, *7* (4), 715−721.
(58) Wang, J.; Li, W.; Yin, W.-J. Passivating Detrimental Dx Centers in $CH_3NH_3PbI_3$ for Reducing Nonradiative Recombination and Elongating Carrier Lifetime. *Adv. Mater.* **2020**, *32* (6), 1906115.
(59) Schlaus, A. P.; Spencer, M. S.; Miyata, K.; Liu, F.; Wang, X.; Datta, I.; Lipson, M.; Pan, A.; Zhu, X. Y. How Lasing Happens in $CsPbBr_3$ Perovskite Nanowires. *Nat. Commun.* **2019**, *10*, 265.

https://doi.org/10.1021/acs.nanolett.1c03142
Nano Lett. XXXX, XXX, XXX−XXX